Acta Chemica Scandinavica, 1998: 52: 261–274
Printed in UK – all rights reserved

ACTA
CHEMICA SCANDINAVICA
ISSN 0904–213X

EPR and ENDOR Simulations for Disordered Systems: The Balance Between Efficiency and Accuracy

Anders Lund and Roland Erickson*

Chemical Physics Laboratory, Department of Physics and Measurement Technology, IFM, Linköping University, S-58183 Linköping, Sweden

Dedicated to Professor Lennart Eberson on the occasion of his 65th birthday

Lund, A. and Erickson, R., 1998. EPR and ENDOR Simulations for Disordered Systems: The Balance Between Efficiency and Accuracy. – Acta Chem. Scand. 52: 261–274. © Acta Chemica Scandinavica 1998.

A method is described to simulate EPR and ENDOR spectra of disordered anisotropic systems with $S=1/2$ or $S=1$ that achieves a suitable balance between computational efficiency and accuracy. Efficiency is obtained by using perturbation theory to treat the hyperfine and nuclear interactions of several (n) nuclei described by the spin-Hamiltonian:

$$H = \mu_B \mathbf{BgS} + \mathbf{SDS} + \sum_{i=1}^{n} (\mathbf{I}_i \mathbf{A}_i \mathbf{S} - g_i \mu_N \mathbf{BI}_i + \mathbf{I}_i \mathbf{Q}_i \mathbf{I}_i)$$

There are no restrictions on the relative magnitude of the hyperfine, quadrupolar, and nuclear Zeeman terms, the electronic Zeeman and fine structure terms ($S=1$), nor on the relative orientation of the principal axes of the tensors.

The latter conditions ensure accuracy as long as the electronic terms dominate. The procedure is particularly useful for organic free radicals and triplet state molecules with several interacting nuclei, where exact methods are expected to be slow. The method has been used to simulate EPR and ENDOR spectra of various disordered systems. A variant of the method which includes microwave saturation has been employed to investigate the power dependence of the intensity of $|\Delta M_I|=1$ spin-flip lines in the EPR spectra of radicals with weakly interacting protons.

1. Introduction

The motivation for simulating EPR and ENDOR spectra is usually the desire to determine hyperfine and quadrupolar couplings. In EPR, simulation is often employed to facilitate interpretation of spectra. Reviews of methods applied to disordered solids have been given in Refs. 1 and 2. In a recent development by Weil and coworkers the spectra were calculated exactly.[3] This is often necessary for ions of transition metals. Methods suitable for EPR simulations of radicals and triplet state molecules were developed by Lefebvre and coworkers.[4,5] A simplifying feature was that the hyperfine and nuclear Zeeman interactions could be treated by perturbation theory. This approximation is utilized in the present paper and in a commercially available programme.[6] However, the latter programme is not applicable to the case with near coincidence of the magnitudes of the hyperfine and nuclear Zeeman terms and therefore cannot account for the 'forbidden', $|\Delta M_I|=1$ transitions which frequently occur in solid-state EPR spectra of organic radicals.[4] A unique feature of the EPR and ENDOR simulation programs developed by us is that the hyperfine, nuclear Zeeman and nuclear quadrupolar interactions are treated with perturbation theory without making any assumptions of the relative magnitudes of the terms. Some results have been published in separate papers.[7–11]

ENDOR spectra are commonly much simpler and fairly straightforward to interpret without simulation in solutions and in single crystals. However, in disordered solids (termed 'powders' in the following) the ENDOR spectrum may not be trivial to interpret. The spectral lines are often broad and the couplings are usually anisotropic. It may be difficult to determine accurately the magnitude and anisotropy of the interactions from the observed spectral features without performing simulations. Attention must also be paid to the orientational selectivity of ENDOR. The EPR spectrum from a powder sample is a superposition of spectral intensities from all possible orientations. Anisotropy of the magnetic interactions results in different resonance conditions for each

* To whom correspondence should be addressed.

orientation. In ENDOR the signal originates from a single position in the EPR spectrum, where the EPR resonance condition is met only for a certain range of orientations. In cases when the EPR spectrum is dominated by a single anisotropic interaction it is sometimes possible to resolve portions that correspond to a single orientation. Rist and Hyde were the first to use the dominating g-anisotropy of Cu and Ag complexes to obtain single crystal-like ENDOR spectra at g-value extrema in the powder EPR spectrum.[12] In free radicals, especially carbon centred species, there is usually no single dominating interaction and it is impossible to obtain such 'single crystal' spectra. Instead, ENDOR spectra are made up of a large number of orientations. Computer simulation can take into account the orientational selectivity and predict the ENDOR spectrum at a specific position in the EPR spectrum. Paired with other EMR methods and the chemical and physical knowledge of the species, ENDOR simulations can facilitate the determination of hyperfine and quadrupolar couplings.

It should be emphasised that the lack of a dominant g-anisotropy in many free radicals can actually be an advantage in some cases. An example is when the single crystal EPR spectrum consists of an odd number of lines and the g-anisotropy is small. In the centre of the corresponding powder spectrum contributions from all orientations will more or less overlap. An ENDOR spectrum obtained at this position will contain contributions from practically all directions. In this case it may be possible to observe all the principal components of, e.g., a hyperfine tensor in the same spectrum. This is demonstrated by the simulations made on both the biphenyl[13] and the naphthalene radical cations.[14]

Several powder ENDOR simulation methods have been described in the literature. Methods to compute ENDOR signals from transition metal complexes obtained at arbitrary field positions have been developed by Hoffman,[15,16] Henderson,[17] Yordanov[18] and their co-workers. In general it is impossible to resolve the g-value extrema of all three principal values in EPR spectra, in order to obtain single crystal-like ENDOR spectra from all three principal directions. Instead signals acquired at general positions in the EPR spectrum must be analysed. Orientational selectivity was taken into account in their theories but ENDOR probabilities were not computed. Kreiter and Hüttermann[19] have described a general theory to calculate powder ENDOR spectra due to arbitrary zero-field splitting, hyperfine and quadrupolar interactions. Magnetic energies and wavefunctions were calculated by exact diagonalization of the spin Hamiltonian. ENDOR transition moments were calculated to zeroth order, neglecting hyperfine enhancement effects. A similar theory has been described briefly by Keijzers *et al.*[20] Powder proton ENDOR of ionic radicals generated on catalyst surfaces has been analysed by Clarkson *et al.*[21] using a theory originally due to Dalton and Kwiram.[22] The method is based on perturbation theory, where transition moments are calculated to first order and relaxation effects are partially taken into account. Orientational selectivity was neglected, as the method assumed that all possible orientations are observed simultaneously in the ENDOR spectrum, independent of the EPR field position.

The method developed by us[23] for ENDOR spectra of $S=1/2$ radicals is based on the same perturbation treatment as that used for EPR spectra.[7,8] The theory differs from the usual perturbation schemes for multiple nuclei in that quadrupolar couplings of the same order as hyperfine coupling can be treated. ENDOR frequencies are calculated neglecting second-order hyperfine contributions. ENDOR transition moments are computed to first order, including quadrupolar interactions and hyperfine enhancement effects. First-order formulas given previously[24,25] neglect quadrupolar interactions. Orientational selection is taken into account in a similar way as in Ref. 17. The treatment is particularly suitable for the simulation of powder spectra with several magnetic nuclei where the exact theory may result in slow calculations.[19,20]

2. Theoretical basis

The simulation programmes are based on similar principles in all cases to treat the electronic, hyperfine and nuclear interactions of the spin Hamiltonian

$$H = \mu_B \mathbf{SgB} + \mathbf{SDS} + \sum_{i=1}^{n} (\mathbf{I}_i \mathbf{A}_i \mathbf{S} - g_i \mu_N \mathbf{B} \mathbf{I}_i + \mathbf{I}_i \mathbf{Q}_i \mathbf{I}_i)$$

$$= H_e + H_f + \sum_{i=1}^{n} (H_{ai} + H_{ni} + H_{qi}) \qquad (1)$$

The principles are: (a) the electronic terms $H_e + H_f$ dominate, but no assumption is made about the relative magnitude, (b) no assumption is made about the relative magnitudes of the H_a, H_n and H_q terms, and (c) the **g**, **D**, **A** and **Q** tensors need not have parallel principal axes. (a) allows perturbation theory to be used. To first order the perturbation from each nucleus can be treated separately, which is computationally efficient in the case of several interacting nuclei. (b) takes automatically into account 'forbidden' transitions which occur, e.g. when the hyperfine interaction is anisotropic and of a similar magnitude as the nuclear Zeeman term. This feature was already included in the classical programme by Lefebvre and Maruani.[4] The treatment here is more general, as it includes the nuclear quadrupole interaction on an equal footing. Thus, the usual assumption[26–28] that the hyperfine interaction is much larger than the quadrupole interaction is not invoked. Consequently, the simulation programmes can be applied to species with large nuclear quadrupole interactions.[7] The condition (c) is applied in several previous simulation programmes, including the initial ones by Lefebvre and coworkers.[4,5] The assumption is necessary, e.g. in the simulation of single crystal or powder spectra of free radical[4] or triplet state molecule spectra[9] containing several inequivalent magnetic nuclei.

The calculation of the line positions and intensities is

carried out by diagonalization of the perturbation matrix $H_i' = H_{ai} + H_{ni} + H_{qi}$ for each nucleus. This treatment is still only first order with respect to H_e ($S=1/2$) and $H_e + H_f$ ($S=1$). The treatment of the perturbation operator is slightly different for the $S=1/2$ and $S=1$ cases. The calculation of the line intensities requires special consideration in the case of ENDOR.[23] A summary of the programs is given in Table 1. Details are given below.

3. First-order $S=1/2$ EPR spectra

It is assumed that the electronic Zeeman term is dominant. The perturbation operator consisting of the hyperfine, quadrupolar and nuclear Zeeman interactions for each nucleus is then[7]

$$H_i' = (\mathbf{I}_i \mathbf{A}_i \mathbf{g} \ell / g) S_u + \mathbf{I}_i \mathbf{Q}_i \mathbf{I}_i - \mu_N g_i B \ell \mathbf{I}_i \tag{2}$$

μ_N is the nuclear magneton, $\ell = \mathbf{B}/B$ is the unit vector along the static field B. The matrix elements of H_i are calculated in an $M_S m_I$ basis. The matrix elements[7] are repeated here for completeness

$$\begin{aligned}
&\langle m|H_a|m\rangle = (M/g) V_z m, \\
&\langle m|H_a|m \pm 1\rangle = (M/g)[I(I+1) - m(m \pm 1)]^{1/2} \\
&\qquad \times 0.5(V_x \pm i V_y)
\end{aligned} \tag{3}$$

where $\mathbf{V} = \mathbf{A} \cdot \mathbf{g} \cdot \ell$.

The non-zero matrix elements of H_b are

$$\begin{aligned}
&\langle m|H_b|m\rangle = -b_z m, \\
&\langle m|H_b|m \pm 1\rangle = -[(I+1) - m(m \pm 1)]^{1/2} 0.5(b_x \pm i b_y)
\end{aligned} \tag{4}$$

where $\mathbf{b} = g_N \mu_N B \ell$.

The matrix elements of H_q are

$$\begin{aligned}
&\langle m|H_q|m\rangle = [3m^2 - I(I+1)] 0.5 Q_{zz} \\
&\langle m|H_q|m \pm 1\rangle = (2m \pm 1)[(I \pm m + 1)(I \mp m)]^{1/2} \\
&\qquad \times 0.5(Q_{xz} \mp i Q_{yz}) \\
&\langle m|H_q|m \pm 2\rangle = \\
&\quad [(I \pm m + 1)(I \mp m)(I \mp m - 1)(I \pm m + 2)]^{1/2} \\
&\quad \times 0.5[0.5(Q_{xx} - Q_{yy}) \pm i Q_{xy}]
\end{aligned} \tag{5}$$

The first-order energies denoted $E'(p_i)$ and $E'(q_i)$ and the eigenstates are computed by diagonalizing the perturbation matrix H_i'. The eigenstates are of the form

$$\begin{aligned}
|p_i\rangle &= \sum_{m=-I}^{+I} a_{pm} |m\rangle \\
|q_i\rangle &= \sum_{m=-I}^{+I} b_{qm} |m\rangle
\end{aligned} \tag{6}$$

To simplify the notation we have deleted the subscript i of the coefficients and the nuclear eigenstates $|m\rangle$. Further the indices p and q are associated with $M_s = 1/2$ and $-1/2$, respectively. Numerical ($I \geqslant 2$) and analytical ($I < 2$) methods to calculate the energies and eigenstates have been described.[7,29]

The EPR transition

$$(1/2, p_1, p_2 \ldots p_n) \leftrightarrow (-1/2, q_1, q_2 \ldots q_n)$$

is denoted by the subscript l. The first derivative powder EPR line shape at the static magnetic field B is approximated by the formula

$$\frac{\mathrm{d}}{\mathrm{d}B} \chi(B) = \int_\varphi \int_\theta \sin\theta \frac{\mathrm{d}}{\mathrm{d}B} \left(\sum_l s(B - B_l) I_l \right) \mathrm{d}\varphi \, \mathrm{d}\theta \tag{7}$$

where s is a Gaussian or Lorentzian function, with a width which may be orientation dependent, see eqn. (22) below. Here φ and θ are the polar angles describing the orientation of the magnetic field. The integration is performed using Gaussian quadrature.[4]

To first order one has

$$B_l = h\nu/g\mu_B - \sum_{i=1}^{n} [E'(p_i) - E'(q_i)]/g\mu_B, \tag{8}$$

where $g^2 = \ell \mathbf{g} \mathbf{g} \ell$.

The expression for the transition probability I_l is

$$\begin{aligned}
&I_l = \mu_B^2 B_1^2 |G|^2 \beta_l / 4 \\
&\beta_l = \prod_{i=1}^{n} \langle p_i | q_i \rangle|^2 \\
&|G|^2 = (\ell_1 \mathbf{g}^2 \ell_1) - (\ell \mathbf{g}^2 \ell_1)^2 / g^2
\end{aligned} \tag{9}$$

ℓ_1 is the unit vector along the direction of the microwave magnetic field B_1. β_l can be computed, using eqn. (6):

$$|\langle p_i | q_i \rangle|^2 = \left| \sum_k (a_{kp})^* b_{kq} \right|^2 \tag{10}$$

The factor $|G|^2$ does not vary appreciably with the orientation for systems with small g-factor anisotropy.[27]

Table 1. EPR and ENDOR programs (in FORTRAN77) available from the authors.[a]

Type	S	Electronic terms	Nuclear terms	Order	Equivalent nuclei	Variable linewidth	Orientation distribution	Power dependence
Anisotropic EPR	1/2	H_e	$H_a + H_n + H_q$	1,2	Yes	Yes	S, P	No
Anisotropic EPR	1/2	H_e	$H_a + H_n + H_q$	1	No	Yes	S, P	Yes
Anisotropic EPR	1	$H_e + H_f$	$H_a + H_n + H_q$	1	No	Yes	S, P	No
Anisotropic ENDOR	1/2	H_e	$H_a + H_n + H_q$	1	No	No	S, P	No
Isotropic EPR	1/2	H_e	H_a	1,2	Yes	No		

[a]The programs, except the last one, are described in the text. Plus signs between terms imply treatment without assumption about their relative magnitudes. Orientation distributions S, single crystal; P, polycrystal, can be treated.

Very good agreement was achieved between experimental and calculated powder spectra, even when the hyperfine and quadrupolar interactions were of comparable magnitude as in the case of the ClSS radical.[8] A typical routine application has been to confirm assignments made by ENDOR by simulation of EPR spectra. In Fig. 1 experimental and simulated spectra obtained from hippuric acid powder X-irradiated at room temperature are shown. The predominant radical R1 with the structure Ph–CO–NH–CH_2 has previously been characterised by single crystal and powder ENDOR.[23,30] The ^{14}N nuclear quadrupole interaction is smaller than the hyperfine term and affects the EPR spectrum only to a minor extent. In contrast to the case with ^{35}Cl and ^{37}Cl in ClSS mentioned above, nuclear quadrupolar couplings with ^{14}N can therefore as a rule not be deduced by fitting of the simulated EPR spectrum to the experimental one. In the ENDOR spectrum of R1 (Fig. 5), however, the effects of the quadrupolar splittings are visible and can be analysed.[23] The second species, R2, is a cyclohexadienyl radical formed by net hydrogen addition to the phenyl ring.[30b]

3.1. Second-order correction to the hyperfine energy. Even though the energies are calculated by diagonalization of the matrix obtained from eqn. (2) the procedure outlined above is still a first-order perturbation treatment with respect to the hyperfine interaction. Second-order corrections have previously been computed under the assumption symbolized by $H_e > H_a + H_n > H_q$ for a system with a single nucleus.[27] No assumption was made on the relative magnitudes of the H_a and H_n terms. Formulae for the special case when in addition $H_a \gg H_n$ have also been given.[26,28]

In the program KVASEC for $S = 1/2$ systems a second-order correction term has been implemented, neglecting the cross terms between different nuclei. The terms in eqn. (1) responsible for the second-order corrections can be written

$$H'' = (\mathbf{IAv})S_v + (\mathbf{IAw})S_w \tag{11}$$

The unit vectors **v** and **w** are perpendicular to the unit vector $\mathbf{u} = \mathbf{g}\ell/g$. One obtains

$$E''\left(\frac{1}{2}p\right) = (4g\mu_B B)^{-1} \sum_{q=1}^{3I+1} \sum_{\alpha\beta=1}^{3} T_{\alpha\beta}\langle p|I|q\rangle\langle q|I_\beta|p\rangle$$

$$E''\left(-\frac{1}{2}q\right) = -(4g\mu_B B)^{-1} \sum_{p=1}^{2I+1} \sum_{\alpha\beta=1}^{3} T_{\alpha\beta}\langle p|I_\alpha|q\rangle\langle q|I_\beta|p\rangle \tag{12}$$

for the $M_s = \pm 1/2$ states, with the definitions

$$T_{\alpha\beta} = (\mathbf{A})^2_{\alpha\beta} - (\mathbf{Au})_\alpha(\mathbf{Au})_\beta + iD_{\alpha\beta}$$

$$D_{\alpha\beta} = \begin{vmatrix} u_1 & u_2 & u_3 \\ A_{1\alpha} & A_{2\alpha} & A_{3\alpha} \\ A_{1\beta} & A_{2\beta} & A_{3\beta} \end{vmatrix}$$

By applying the closure relation and noting that $D_{\beta\alpha} = -D_{\alpha\beta}$ one can show that the right hand expressions are real quantities, as expected. We have not succeeded, however, to verify by analytical methods that the expressions (12) are equivalent to the formulae given in Refs. 26–28 when the condition $H_a + H_n > H_q$ applies. The equations have therefore been tested numerically by comparing the line positions and intensities obtained by diagonalizing the full Hamiltonian with those of the present theory for the system shown in Table 2. The agreement for the line positions is good except for a few lines of low intensity. The intensities agree very well.

3.2. Second-order effects from several nuclei. Two cases which are of practical importance are the second-order hyperfine splittings due to equivalent nuclei and the effect of a large hyperfine splitting on a small one. In a first approximation, the first case has been treated as in isotropic systems.[31] The nuclear spins I are coupled to obtain the resultant spin angular momentum I_r. The number of times the value I_r is obtained (multiplicity M_r) can be calculated analytically for the $I = 1/2$ case. An algorithm has been implemented in the programs described here to obtain the I_r and M_r values for any nuclear spin. The Hamiltonian has no elements which are off-diagonal in I_r, and one can therefore obtain the energies and add the spectra of each I_r weighted by M_r. This procedure has been applied to simulate the spectrum of Ag_3^{2+} in zeolite (Fig. 2). The experimental spectrum contains in addition signals from other species, but the agreement of the parts attributed to $^{109}Ag_3^{2+}$ with the simulation is good. The agreement with a simulation based on exact theory is also satisfactory.[32] This gives support for the correctness of the formulae (12) for second-order corrections for the special case of axial

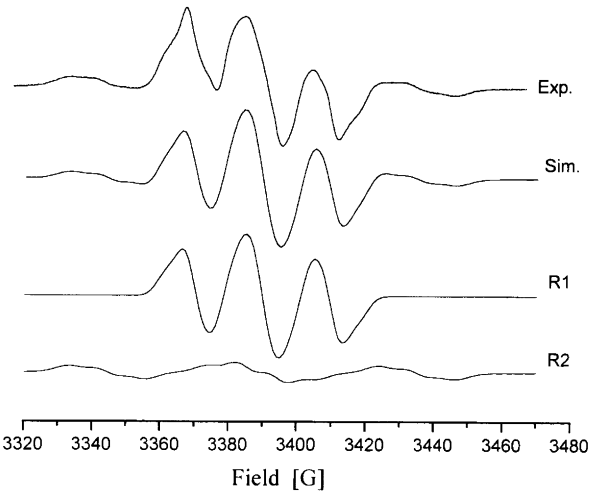

Fig. 1. EPR powder spectra of radicals in X-irradiated hippuric acid (a) experimental, (b) simulated spectrum composed of the components R1 = Ph-CO-NH-$\dot{C}H_2$ and R2 = cyclohexadienyl radical. Parameters for simulation were taken from Refs. 23 and 30.

Table 2. Line positions and intensities for a radical with g_x= 2.0003, g_y=2.024, g_z=2.0215 and with a ^{81}Br nucleus with A_x=100 G, A_y=−20 G, A_z=−32 G, Q_x=−9.82 G, Q_y=−9.82 G and Q_z=19.64 G at a microwave frequency of 9500 MHz.

	Position/G		Intensity	
Orientation	2nd order	Exact	2nd order	Exact
$B \parallel X$	3229.7	3229.5	0.1911	0.1910
	3314.4	3314.4	0.0589	0.0590
	3329.8	3329.8	0.1935	0.1937
	3371.4	3371.3	0.0589	0.0590
	3419.3	3419.4	0.0565	0.0562
	3456.1	3456.1	0.1911	0.1910
	3466.4	3466.4	0.0565	0.0563
	3555.9	3556.0	0.1935	0.1938
$B \parallel Y$	3281.6	3282.0	0.0225	0.0195
	3298.0[a]	3299.1	0.0192	0.0223
	3331.9	3331.9	0.2274	0.2304
	3350.7	3351.0	0.2274	0.2303
	3351.5	3351.8	0.2308	0.2278
	3371.1	3370.8	0.2308	0.2278
	3401.1	3401.0	0.0226	0.1097
	3424.6[a]	3423.5	0.0192	0.0221
$B \parallel Z$	3308.4	3308.9	0.2500	0.2501
	3338.8	3339.0	0.2500	0.2498
	3370.8	3370.7	0.2500	0.2499
	3404.4	3403.9	0.2500	0.2501

[a]Lines with the biggest difference between the second-order and exact positions.

symmetry. The quadrupolar interaction for $I>1/2$ nuclei is not taken into account in the algorithm, however.

The other case of practical interest involves the shift of transition frequencies in ENDOR or field positions in EPR due to cross-terms to second order between non-equivalent nuclei. The cross-term for a system with two nuclei is

$$E^x\left(\frac{1}{2}p_1p_2\right) = (2g\mu_B B)^{-1} \times \left(\sum_{ij=1}^{3} T_{ij}^x \langle p_1|I_i^{(1)}|p_1\rangle\langle p_2|I_j^{(2)}|p_2\rangle\right) \quad (13)$$

with the definitions

$$T_{ij}^x = (\mathbf{A}^{(1)}\mathbf{A}^{(2)})_{ij} - (\mathbf{A}^{(1)}\mathbf{u})_i(\mathbf{A}^{(2)}\mathbf{u})_j$$

The different nuclei are denoted by superscripts (operators, matrices) and subscripts (wavefunctions) 1 and 2.

Equation (13) involves the computation of $\langle p_\alpha|I_i^{(\alpha)}|p_\alpha\rangle$ over the states p_α given by eqn. (7) for the two nuclei (α=1 and 2). In the present implementation the computation of the matrix elements is done in a loop over the nuclei without storage of preceding elements. The second-order cross-term between two nuclei can therefore not be computed. The cross-term has a form differing from that obtained under the condition $H_a > H_q$.[28] The correctness of eqn. (13) therefore needs to be established before it can be applied. The neglect of the cross-term is of significance especially in the simulation of ENDOR spectra from ligand nuclei of transition metal ions like Cu^{2+}, where the central nucleus has a

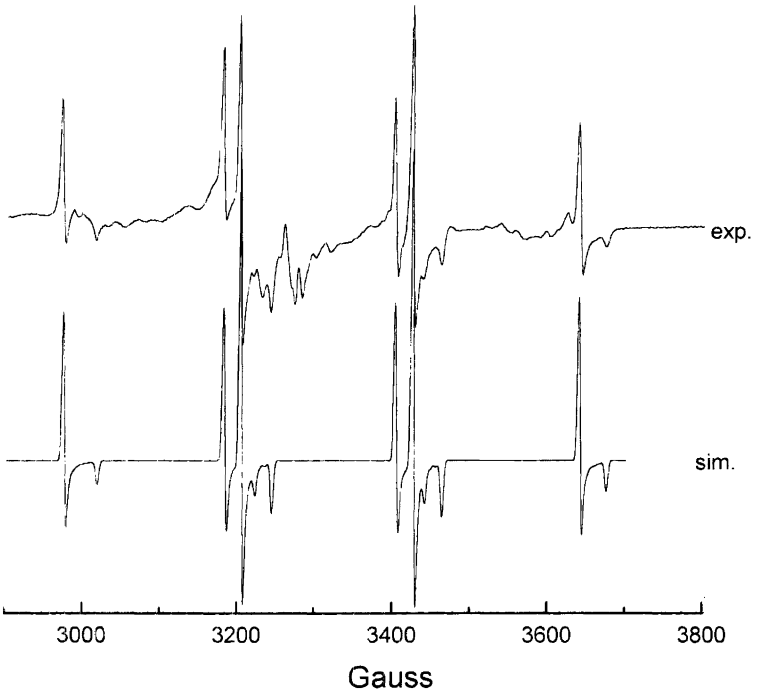

Fig. 2. Experimental and simulated spectra of Ag_3^{2+} in zeolite showing second-order hyperfine splittings due to three equivalent ^{109}Ag nuclei. The parameters are $g_\parallel$=1.958, $g_\perp$=1.981, $A_\parallel$=218.8 G, $A_\perp$=221.6 G, linewidth=4 G peak-peak of first derivative. The experimental spectrum was provided by Prof. J. Michalik.

large anisotropic hyperfine coupling. The cross-term gives rise to frequency shifts which cannot be accounted for with the ENDOR simulation programme described below. From eqn. (13) follows that cross-terms do not appear when the two nuclei have isotropic hyperfine couplings. This is in accordance with the result in Ref. 28. An implicit assumption in the treatment here and in Ref. 28 is that the nuclei are not equivalent. This case is treated separately in our programs for the special case that the nuclear quadrupole interaction is negligible. The case with equivalent nuclei having large quadrupole interactions cannot be treated with the programme presented here.

4. Calculation of EPR spectra of $S=1$ molecules

Simulations of $S=1$ EPR spectra excluding hyperfine and nuclear interactions were first performed by Kottis and Lefebvre.[5] They calculated exactly the transition fields and intensities from the electronic Zeeman, H_e, and zero-field splitting, H_f, terms. In our implementation the hyperfine, nuclear Zeeman and quadrupole terms were taken into account under similar conditions as for the $S=1/2$ case, i.e. $H_e+H_f \gg H_a+H_n+H_q$.[10] No assumption is made of the relative magnitudes of the terms within the two groups or about the orientation of the tensor axes. The treatment follows closely the $S=1/2$ case and only the differences are highlighted.

Field strength: The field strengths at which the transitions occur for a constant microwave frequency are calculated from an equation[10] of the form

$$F(B,\Delta) = -4g^6(\mu_B B)^6 + (12g^4 d + 9g^4\Delta^2 + 27e^2)(\mu_B B)^4 - [6g^2(\Delta^2+2d)(\Delta^2+d) + 54ef](\mu_B B)^2 + (\Delta^2+4d)(\Delta^2+d)^2 + 27f^2 = 0, \quad (14)$$

where $g^2=\ell\mathbf{g}^2\ell$, $d=D_1D_2+D_1D_3+D_2D_3$, $e=-\ell\mathbf{gDg}\ell$, $f=-D_1D_2D_3$, and $\Delta=h\nu$. D_1, D_2, and D_3 are the principal elements of the zero-field splitting tensor and $\ell=\mathbf{B}/B$ is specified with respect to the principal axes of the zero-field splitting tensor.

Transformation of coupling tensors: The condition that the field equation is expressed in the zero-field splitting coordinate system makes it necessary to transform the principal axes and the field vector as follows

$$\mathbf{u}'=\gamma\cdot\mathbf{u} \quad (15)$$

where γ is the matrix of direction cosines of the D tensor, $\mathbf{u}$ is a vector in the laboratory system and $\mathbf{u}'$ the corresponding vector in the D-axis system.

Transition intensity between electronic states α and β: The electronic part of the Hamiltonian is diagonalized at each of the fields (3 in general) obtained from eqn. (14). The resulting state vectors $\mathbf{C}_\alpha$ and $\mathbf{C}_\beta$ were obtained in the T basis that diagonalises the zero-field Hamiltonian. In (10) the intensity $I_{\alpha\beta}$ was computed under the assumption that the g-factor anisotropy could be neglected. It was further implicitly assumed that the same expression was valid for the single crystal case as for a disordered system. In connection with the development of the ENDOR programme a distinction between the two cases became necessary.[23] The intensities for the single (s) and polycrystal cases (p) are

$$I_{\alpha\beta}^{(s)} = \mu_B^2 B_1^2 |\mathbf{C}_\alpha^* \times \mathbf{C}_\beta \cdot \mathbf{g}\ell_1|^2 \quad (16a)$$

$$I_{\alpha\beta}^{(p)} = \tfrac{1}{2}\mu_B^2 B_1^2 \{|\mathbf{gC}_\alpha^* \times \mathbf{C}_\beta|^2 - |(\mathbf{C}_\alpha^* \times \mathbf{C}_\beta)\cdot\mathbf{g}\ell)|^2\} \quad (16b)$$

ℓ_1 is a unit vector parallel to the microwave magnetic field B_1. B_1 is assumed to be linearly polarised perpendicular to the static magnetic field. In practice the g-anisotropy of organic $S=1$ molecules is negligible, and the spectrum shape is unaffected by the intensity factor in single crystals. Therefore, in the implementation eqn. (16b) is used. With an isotropic g the formula becomes the same as in Ref. 10.

Hyperfine interaction: Because of the zero-field term a transformation of the hyperfine term like in the $S=1/2$ case cannot be performed. The calculation is therefore performed with the original operator. The nonzero matrix elements of the hyperfine term are

$$\langle\alpha, m|\mathbf{S}\cdot\mathbf{A}\cdot\mathbf{I}|\alpha, m\rangle = V_z^{\alpha\alpha} m,$$

$$\langle\alpha, m|\mathbf{S}\cdot\mathbf{A}\cdot\mathbf{I}|\alpha, m\pm 1\rangle = 1/2[I(I+1)-m(m\pm)]^{1/2}(V_x^{\alpha\alpha} \pm iV_y^{\alpha\alpha}) \quad (17)$$

where $V_j^{\alpha\alpha}$ is obtained by putting $\beta=\alpha$ in the expression

$$V_j^{\alpha\beta} = -i\sum_{i=1}^{3} A_{ij}(\mathbf{C}_\alpha^* \times \mathbf{C}_\beta)_i \quad (18)$$

(Note that $\mathbf{C}_\alpha$ is a complex vector so that $V_j^{\alpha\alpha}$ is not zero.) The matrix elements of the quadrupole and nuclear Zeeman terms are given by eqns. (4) and (5).

The positions of the hyperfine lines are obtained as

$$\Delta B_{pq} = -\Delta W_{pq}/(\mathrm{d}W/\mathrm{d}B) \quad (19)$$

where ΔW_{pq} is the energy separation for the transition $(\alpha p)\leftrightarrow(\beta q)$.

The minus sign in eqn. (19) accounts for the fact that a positive energy difference corresponds to a negative field shift. The quantity $(\mathrm{d}W/\mathrm{d}B)$ is the factor which converts energy separations into field shifts. For values of zero-field splittings much less than $g\mu_B B$ we have $(\mathrm{d}W/\mathrm{d}B=g\mu_B)$. In the general case one has to evaluate

$$(\mathrm{d}W/\mathrm{d}B) = -(\partial F/\partial B)/(\partial F/\partial\Delta) \quad (20)$$

at

$$B = B_{\alpha\beta}.$$

The resulting formula, see Ref. 10, obtained by differentiation of eqn. (14) is implemented in the program.

The intensities of the hyperfine lines are computed as in the $S=1/2$ case. Several nuclei are treated by using a product basis of nuclear spin functions. The matrix of nuclear interactions is block diagonal with respect to the nuclei to first order. Consequently, as in all other programs presented here, each nucleus can be treated separately.

This program was applied in the analysis of the trimethylene methane data.[9]

This $S=1$ molecule is characterized by an isotropic factor, $g=2.002$, $D=0.0248\ \mathrm{cm}^{-1}$, $|E|\leqslant 0.0003\ \mathrm{cm}^{-1}$, and a hyperfine structure with six protons with $\mathbf{A}=(-14, -38, -26)$ MHz. The principal axes of the proton coupling tensors are related by a threefold symmetry axis of the molecule. Owing to the relatively small zero-field splitting the spectrum is characterized by two strong $\Delta M_s=1$ transitions and a weak $\Delta M_s=2$ transition. The spectrum consists of $3\times 4^6=8192$ transitions. An algorithm which lumps together degenerate transitions and eliminates lines weaker than a treshold value has been implemented to reduce the computation time. As shown before the hyperfine patterns of the $M_s=1\rightarrow 0$ and $M_s=0\rightarrow -1$ transitions differ.[33] By simulation of single-crystal spectra, the signs of the hyperfine tensor components could be determined relative to the sign of the fine structure.[9] The $\Delta M_s=1$ powder spectrum in Fig. 3a took less than 1 h to compute on a modern PC (Pentium 200 MHz processor). As can be seen by comparing the simulation for $D>0$ with that for $D<0$ a difference is also obtained in the powder. As shown before the correct assignment is $D>0$.[9] The $\Delta M_s=2$ part is less time demanding. A simulated spectrum is given in Fig. 3b. The spectrum compares favourably with that experimentally obtained. To our knowledge $S=1$ powder spectra of such complexity as from TMM have not been simulated before. The program was designed to handle also the cases with a quadrupolar term comparable to the hyperfine and nuclear Zeeman terms. Systems of this type containing chlorine and bromine have been investigated by ODMR.[34] We have not attempted to simulate the spectra, however.

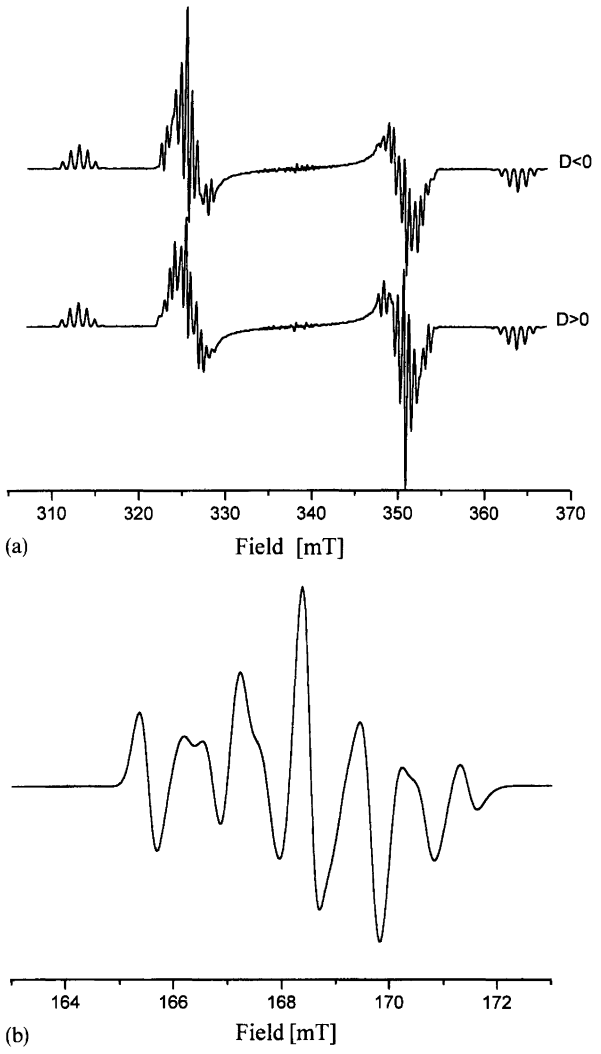

Fig. 3. (a) Simulated $\Delta M_s=1$ EPR spectrum of trimethylenemethane, $C(CH_2)_3$, in polycrystalline methylenecyclopropane, with $D>0$ and $D<0$, respectively. Parameters were taken from Ref. 9. (b) Simulated $\Delta M_s=2$ EPR spectrum of $C(CH_2)_3$ in polycrystalline methylene cyclopropane. See Ref. 52 for an experimental spectrum.

5. Simulation of microwave power dependence of satellite lines

The radiation dose can be measured from the yield of free radicals by EPR. The alanine EPR dosimeter has gained general acceptance.[35] In the so-called stable alanine radical (SAR) the deaminated radical species $CH_3C^{\cdot}HCOO^-$ dominates the spectrum. The radical interacts weakly by dipolar interaction with three protons of an adjacent alanine molecule.[36] This gives rise to $|\Delta M_I|=1$ spin flip lines.[37] In the absence of microwave saturation the signal intensity depends linearly on $P^{1/2}$, where P is the applied microwave power. To obtain high sensitivity relatively high microwave power is often applied. The main lines normally saturate at lower power than the satellite lines. At high power the intensity of the satellite lines therefore grow in comparison with the main lines. Most computer simulation routines available today do not take this dependency into account. A phenomenological method[11] has therefore been devised and implemented in one of the computer codes described in this paper. The implementation is based on a theory of continuous saturation by the microwave field.[38] In the case when all the lines are well resolved, the EPR absorption of a line centred at B_0 of intensity β_0 is

$$S_H(B, B_1)=C_1B_1\frac{\beta_0 g_H(B-B_0)}{1+C_2\beta_0B_1^2(B-B_0)}. \tag{21}$$

The equation applies to the homogeneous saturation case.

Inhomogeneous contributions give rise to additional broadening. The EPR absorption can be calculated analytically in the limiting case when the inhomogeneous line width greatly exceeds the line width of the spin packet.[39,40] It is customary to use Lorentzian and Gaussian functions for the homogeneous and inhomogeneous line shapes g_H and g_I. Under these assumptions one has for a line centred at B_0 of intensity β_0

$$S_I(B, B_1)=K_1B_1\beta_0\frac{g_I(B-B_0)}{(1+K_2\beta_0B_1^2)^{1/2}} \tag{22}$$

Constants K_1 and K_2 and C_1 and C_2 are proportionality

constants. The forms of expressions (21)–(22) suggest a phenomenological equation for the effect of saturation in a spectrum composed of L lines

$$S(B, P) = K_1 P^{1/2} \sum_{l=1}^{L} \frac{\beta_l g(B - B_l)}{(1 + \beta_l P/P_0)^{\alpha}} \tag{23}$$

Experimentally, the linewidth of the SAR depends on the orientation.[11] It is therefore assumed that the shape function g has an orientation dependent width w given by the equation

$$w^2 = \ell(\mathbf{T})^2 \ell \tag{24}$$

$\mathbf{T}$ is a tensor specified by its principal values and the direction cosines of the principal directions. The formula agrees with that of Pilbrow when the g-anisotropy is neglected.[2]

For the stable alanine radical (SAR) a modified formula (23) had to be employed to predict correctly the relative intensities of the main lines at high microwave power. For the main lines a saturation factor $(1+P/P_0)^{-\alpha}$ was used in place of the factor $(1+\beta_l P/P_0)^{-\alpha}$ used for the satellite lines. The parameter P_0 was estimated from the saturation behaviour of the experimental spectra. The parameter α was chosen empirically in the range $0.5 \leqslant \alpha \leqslant 1.0$ to conform with the extreme cases of completely inhomogeneous and homogeneous broadening.

Except for the saturation factor, the expression for the spectrum is identical to that of the unsaturated case. This factor accounts for the difference in saturation between lines of different transition probability β_l. Satellite lines due to nuclear 'spin flip' transitions occur when the hyperfine coupling is strongly anisotropic and of comparable magnitude to the nuclear Zeeman coupling. These 'forbidden' lines will not saturate as easily as the main lines. Any program which takes forbidden transitions into account may be employed, e.g. the classical program by Lefebvre and Maruani.[4] Our treatment is based on the theory presented above for the $S=1/2$ case.

In Ref. 11 simulations for single crystal and polycrystalline SAR were obtained at different microwave powers. The satellite lines became of comparable intensity to the main lines in the experimental and simulated spectra at high microwave power. The radical trapped after X-irradiation at room temperature of ammonium tartrate is $^{-}$OOC–C$^{\cdot}$(OH)–$^{\cdot}$CH(OH)–COO^{-}.[41] As judged from the magnitudes of the hyperfine interactions with the β and hydroxy protons, spin flip lines are to be expected also in this case. The simulations in Fig. 4 support this prediction. Experimental studies of this system are in progress in our laboratory in search of a sensitive EPR dosimeter.

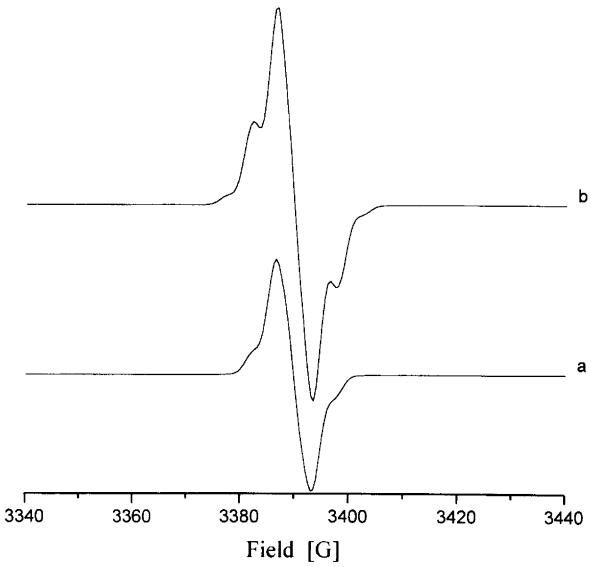

Fig. 4. Simulated first derivative X-band spectra at different microwave power levels of X-irradiated ammonium tartrate. The simulated spectra are calculated using tensor data for the -OOC-$^{\cdot}$C(OH)-CH(OH)-COO^{-} in Ref. 41: (a) unsaturated spectrum, $P=0.1$ mW; (b) saturated spectrum, $P=64$ mW, $P_0=0{,}5$ mW, $\alpha=0.7$ [see eqn. (23) for explanation of parameters].

6. First-order $S=1/2$ ENDOR spectra

6.1. Calculation of ENDOR transition frequencies. The first-order theory for $S=1/2$ EPR forms the basis for calculation of corresponding ENDOR transition frequencies and intensities. The perturbation (11) gives no energy contribution to first order and the ENDOR transition frequency between two nuclear eigenstates $|h_i\rangle$ and $|k_i\rangle$, $\Delta M_s=0$, is obtained as

$$f_{h_i k_i} = |E'(h_i) - E'(k_i)| \tag{25}$$

where $|h_i\rangle$ and $|k_i\rangle$ belong to the same M_s-manifold, i.e. either the $|p_i\rangle$ or the $|q_i\rangle$-manifolds defined in eqn. (6). Note that in general the eigenstates are mixtures of nuclear spin states. $E'(h_i)$ and $E'(k_i)$ are the first-order nuclear energies of the two states, defined in section 3.

The neglect of higher-order terms is justified for hyperfine interactions (hfi) smaller than 40–50 MHz, measured at high magnetic field. For larger interactions the second-order corrections of section 3.1 can be applied. However, they are not implemented in our ENDOR program, since the major application is to measure small hfi unresolved in EPR spectra. Neither are second-order terms due to cross-terms between different nuclei included in eqn. (25). Second-order split/shifts due to magnetically equivalent nuclei with small hfi are generally too small to be resolved in broad powder ENDOR lines. For the four equivalent protons of naphthalene$^{\cdot+}$, described in Ref. 14, each first-order resonance line is shifted and split into four lines. The split/shift can be calculated with a formula given by Iwasaki.[27] The largest second-order splitting, which occurs for the hyperfine tensor component of -7.9 MHz, is ca. 0.023 MHz. Since the linewidth is 0.6 MHz the splitting is not resolved. The second-order splitting might be noticeable for larger hfi measured in single crystals. Splittings/shifts of up to 0.2 MHz have

been observed by Toriyama and coworkers[24] for methyl protons with a hfi of ca. 60 MHz in a single crystal of $CH_3COOLi \cdot 2H_2O$. A more important effect is that of second-order terms in small hfi in the presence of nuclei with very large hfi, as described in section 3.2. These are not taken into account in eqn. (25), but if necessary eqn. (13) can be applied.

6.2. Calculation of ENDOR transition moments. The probability for a radiation-induced transition in ENDOR between nuclear spin states $|h_i\rangle \Leftrightarrow |k_i\rangle$, $\Delta M_s = 0$, for a nucleus with spin I_i, is given by Fermi's golden rule:[24,42]

$$P = 2\pi W^2 \rho(\omega) \tag{26}$$

where $\rho(\omega)$ is the frequency distribution function of the radiation and

$$W^2 = |\langle \Phi(M_s, \underline{h}, h_i)|\mathbf{B}_2 \cdot (\mu_B \mathbf{gS} - \sum_{j=1}^{n} g_j \mu_N \mathbf{I}_j) \times |\Phi(M_s, \underline{h}, k_i)\rangle|^2 \tag{27}$$

The label $\underline{h}$ is an abbreviation for the states $h1, \ldots, h_{i-1}, h_{i+1}, \ldots, h_n$ of the nuclei which remain unchanged in the transition. The first-order eigenfunctions for $M_s = +1/2$ are given by:

$$|\Phi(+1/2, h_1, \ldots, h_n)\rangle = |+1/2, h_1, \ldots, h_n\rangle + \sum_{q_1 q_2 \cdots q_n} \frac{\langle -1/2, q_1, \ldots, q_n | \sum_{i=1}^{n} H_i'' | +1/2, h_1, \ldots, h_n\rangle}{+g\mu_B B} \times |-1/2, q_1, \ldots, q_m\rangle \tag{28}$$

where the outer summations runs over all nuclear states $|q_i\rangle$ in $|-1/2, q_1, \ldots, q_n\rangle = |-1/2\rangle |q_1\rangle |q_2\rangle \ldots |q_n\rangle$. The labels in Φ $(+1,2, h_1, \ldots, h_n)$ identify the state labels of the leading term in the first-order expression. Energy terms smaller than the order of $g\mu_B B \times 10^{-2}$, caused by the nuclear interactions H_i', have been neglected in the denominator. The corresponding expression for $|\Phi(-1/2, q_1, q_2, \ldots, q_n)\rangle$ is obtained by exchanging places of all h_i and q_i, and plus and minus signs in formula (28). In the special case of a single nucleus (27) becomes

$$W^2 = |\langle \Phi(M_s, h)|\mathbf{B}_2 \cdot (\mu_B \mathbf{gS} - g_N \mu_N \mathbf{I})|\Phi(M_s, k)\rangle|^2. \tag{29}$$

The use of first-order wavefunctions is important to predict ENDOR transition moments properly. As described by Schweiger and Günthard,[25] first-order moments show good performance, whereas zero-order formulas may differ from exact values by orders of magnitude. The transition moment in a single crystal is, in general, anisotropic and depends on the orientation of the molecule relative to the static and the RF field.[23–25] In powders transition moments require integration over the directions of both the static and the RF field, as discussed further below. Zero-order transition moments only show orientational dependence when the static field is oriented away from the principal axes of the hyperfine tensor.[42] Further, zero-order calculations are insufficient to predict hyperfine enhancement effects.

The Hamiltonian operator used in eqn. (27) represents the interaction between the RF field, $\mathbf{B}_2$, and the electron and nuclear magnetic moments. The square of the matrix element W, the transition moment, selects the allowed transitions and predicts the relative intensities, neglecting relaxation effects. The overall intensity of an ENDOR line is determined by the balance between different nuclear and electronic relaxation pathways. A model of relaxation in solution ENDOR has been worked out by Freed and co-workers.[43] However, only a few experimental investigations[44] have been made of relaxation in ENDOR of solid samples at low temperatures. Further, the detailed knowledge of all relaxation rates needed in a theoretical model makes the calculations complex and has not been incorporated in the present method. The use of transition moments to predict intensities while neglecting relaxation can still in many cases give a sufficiently good fit to enable a spectral interpretation, as demonstrated in Refs. 13, 14 and 23.

6.3. Formulae of ENDOR transition moments in single crystals. The squared transition moment, eqn. (27), calculated with the first order wavefunctions (28) is given by[23]

$$W^2 = (B_2/B)^2 |\langle h|\mathbf{ICr}|k\rangle|^2 \tag{30}$$

for a transition between nuclear states $|h\rangle \Leftrightarrow |k\rangle$, $\Delta M_s = 0$ of a nucleus with spin I in a single crystal. The nuclear index i has been dropped to simplify the formula. The term C is defined in Table 3, where symbol A is the hyperfine matrix, 1 is the identity matrix, ν_N is the nuclear Larmor frequency. Symbols B_2 and $\mathbf{r}$ are the strength and direction of the RF field $\mathbf{B}_2$, which is oriented perpendicular to the static field direction ℓ. The static field $\mathbf{B}$ has the strength B.

Equation (30) covers the case of strong nuclear quadrupolar interactions (nqi), compared to the hyperfine coupling, when the usual $\Delta m_I = \pm 1$ selection rule breaks down. In Table 3 the equation is collected as eqn. (a) together with formulae neglecting nqi. With zero quadrupolar interaction eqn. (30) can be simplified to an analytical formula, eqn. (b) of Table 3, first reported by Toriyama *et al.*[24] First-order formulae under similar assumptions have also been reported by Dalton and Kwiram.[22] Without nqi the nuclear spins are quantised along the direction:

$$\mathbf{k} = \mathsf{C}\ell / |\mathsf{C}\ell|. \tag{31}$$

The nuclear wavefunctions are then eigenstates $|m_I\rangle$ to the operator $I_k = \mathbf{I} \cdot \mathbf{k}$. Introducing two orthogonal unit vectors $\mathbf{p}$ and $\mathbf{q}$, which are perpendicular to $\mathbf{k}$, the operator $\mathbf{ICr}$ in eqn. (30) can be expanded as:

$$\mathbf{ICr} = \mathbf{I} \cdot \mathbf{k}(\mathbf{kCr}) + \mathbf{I} \cdot \mathbf{p}(\mathbf{pCr}) + \mathbf{I} \cdot \mathbf{q}(\mathbf{qCr}) \tag{32}$$

Inserting eqn. (32) into the general eqn. (27) and using

Table 3. Square of first-order ENDOR transition moments, W^2, in multiples of $(B_2/B)^2$ in a single crystal for a transition between nuclear states $|h\rangle \Leftrightarrow |k\rangle$, $\Delta M_s = 0$ of a nucleus with spin I.

Equation number and application	W^2 (in multiples of $(B_2/B)^2$	Refs.
a. Arbitrary A, Q Modest g-anisotropy[a]	$\lvert\langle h\rvert \mathbf{ICr} \rvert k\rangle\rvert^2$	23
b. Q = 0 Arbitrary A Modest g-anisotropy[a]	$f\pm^2[\mathbf{rCCr} - (\mathbf{rCC}\ell)^2/(\ell\mathbf{CC}\ell)]$	23, 24,[b] 25[b]
c. Q = 0 **B** // principal axis z of A $\mathbf{B}_2$ // principal axis **x** of A Isotropic g	$f\pm^2 \nu_N^2[1 - M_s A_x/\nu_N]^2$	23, 24,[b] 25,[b] 45[b]
d. Q = 0 Arbitrary A, g	$f\pm^2[\mathbf{rCCr} - (\mathbf{rC}\ell)^2 + (\mathbf{rC}\ell - \mathbf{rgg}\ell\nu_N/g^2)^2 - (\mathbf{rCC}\ell - \mathbf{rgg}\ell\ell\mathbf{C}\ell\nu_N/g^2)^2/(\ell\mathbf{CC}\ell)]$	25[c]

Notation:

$\mathbf{C} = M_s\mathbf{Ag}/g - \nu_N\mathbf{1}$

$f\pm^2 = (I(I+1) - m_I(m_I \pm 1))/4$

Formulas for W^2 when $Q = 0$, eqns. (3b)–(3d) apply to $|h\rangle = |m_I \pm 1\rangle$, $|k\rangle = |m_I\rangle$. Wavefunctions $|m_I\rangle$ are eigenfunctions of the operator $I_k = I \cdot \mathbf{k}$, where $\mathbf{k} = \mathbf{C}\ell/|\mathbf{C}\ell|$

[a]The g-anisotropy is here defined as modest if g fulfills: $(1/g^2)\mathbf{rgg}\ell \ll 1$ when $\mathbf{r} \cdot \ell = 0$.[b]Corresponding expressions have been published in Refs. 24 and 25 [eqn. (b)] and 24, 25 and 45 [eqn. (c)].[c]Adapted to the notation of this paper.

the identity

$$\mathbf{rCCr} = (\mathbf{kCr})^2 + (\mathbf{pCr})^2 + (\mathbf{qCr})^2 \qquad (33)$$

eventually gives eqn. (b) in the table. Equation (a) and hence also (b) in Table 3 assumes that the g-anisotropy is small enough that the relation $(1/g^2)\mathbf{rgg}\ell/g^2 \ll 1$ is valid. Here **r** is assumed to be perpendicular to ℓ, the configuration found in conventional ENDOR spectrometers. The relation is fulfilled for most free radicals since their g-anisotropy amounts only to a few percent of the isotropic value.

For large g-anisotropy but neglecting quadrupolar interactions Schweiger and Günthard[25] have derived a very accurate formula, given in our notation as eqn. (d) in Table 3. The equation shows perfect agreement with exact numerical calculations even for g-anisotropies exceeding 30% of the isotropic value.[25] Inspection of the equation gives that it agrees with eqn. (b) if $\mathbf{rgg}\ell/g^2$-terms are neglected. For g-anisotropies up to a few percent these terms have negligible effect. For a larger anisotropy of 10% eqn. (b) is, as a rule of thumb, accurate to within 1–2% of the more exact value of eqn. (d) in Table 3. Table 5 shows a comparison of transition moments calculated for a methylene proton in Cu^{II}-doped α-glycine which has the principal g-values, 2.0434, 2.0715 and 2.2644[45] (Table 4). The relative difference between the two equations varies from 0.4% up to 1.5% of the 'exact' value. The largest discrepancy occurs for the $M_s = +1/2$ transition with **B** along crystal axis **b** and $\mathbf{B}_2$ along **a**.

6.4. Properties of ENDOR transition moments. Two important properties of ENDOR transition moments in solids are the so called hyperfine enhancement effect, and the dependence of the orientation of the RF field.[23–25,46]

Table 4. The g and hyperfine tensors[a] of the methylene proton 1 in Cu^{II}-doped α-glycine single crystal obtained at 4.2 K.

Tensor	Principal value[b]	Direction cosines[c]		
g	2.0434	−0.234	0.652	0.721
	2.0715	−0.718	0.379	−0.581
	2.2644	0.656	0.654	−0.378
A_1	6.35	0.561	0.776	−0.288
	1.99	−0.661	0.211	−0.721
	1.14	−0.499	0.595	0.631

[a]The g-tensor and the methylene proton hyperfine tensor data were taken from Ref. [46]. [b]Hyperfine values in MHz. [c]With respect to axes **a**, **b** and **c**′, see Ref. 46.

Table 5. Comparison of squared first-order ENDOR transition moments, W^2, (arbitrary units) of proton 1 in a single crystal of Cu^{II}-doped α-glycine.

$\mathbf{B}_2$ parallel to axis	**B** parallel to axis	M_s	W^2 according to Table 3, eqn. (b), neglecting $\mathbf{rgg}\ell$-terms	W^2 according to Table 3, eqn. (d), including $\mathbf{rgg}\ell$-terms
a	**b**	+	16.05	16.30
		−	26.10	25.83
a	**c**′	+	16.31	16.38
		−	26.34	26.25
b	**a**	+	15.98	16.21
		−	26.30	26.05
b	**c**′	+	16.01	16.13
		−	26.32	26.18
c′	**a**	+	17.20	17.33
		−	25.20	25.05
c′	**b**	+	16.97	17.09
		−	24.98	24.86

Both effects can be illustrated by considering a simple case first discussed by Whiffen.[46] The g factor is assumed to be isotropic and the quadrupolar interaction to be zero. The static and the RF fields are directed parallel to two principal axes, say **z** and **x**, of the hyperfine tensor A; i.e. ℓ//**z** and **r**//**x** In this case eqns. (a) and (b) of Table 3 will become eqn. (c), first given by Whiffen.[46] The term A_x is the principal component of A along **x**. The enhancement factor $1-M_sA_x/\nu_N$ reflects that the hyperfine field produced at the nucleus gives an important contribution to the RF field in driving the nuclear transitions. The effect, first recognised by Abragam,[47] is commonly known as 'hyperfine enhancement'. The enhancement factor would be equal to one if the interaction between the electron and the RF field would be neglected in the transition moment eqns. (27) and (29). The enhancement effect can be very large for nuclei with small magnetic moments, such as ^{14}N. For nuclei with large magnetic moments, such as protons, the effect is less pronounced. However, it can still cause unexpectedly low intensities for the low-frequency transition, making it difficult to detect in a powder sample, as illustrated by the *para* protons of the biphenyl radical cation studied in Ref. 13. The hyperfine tensor has the principal components A_x, A_y, A_z: −26.9, −7.9 and −18.3 MHz. For the assumed ℓ and **r** directions eqn. (c) gives the values 3.7 ($M_s=+1/2$) and 0.0 ($M_s=-1/2$), making the latter transition difficult to detect.

The dependence on the RF field orientation in the enhancement factor is reflected in eqn. (c) in Table 3 by the term A_x, the component of A along $\mathbf{B}_2$. The frequency and the probability of the transition are thus governed by different components of the hyperfine tensor. This is a general property of ENDOR moments in solids and for a fixed orientation of **B** it is a function of the orientation of $\mathbf{B}_2$ in the plane perpendicular to **B**. For the *para* protons discussed above the squared enhancement factor for **B**//**z** will vary between 1.6 and 3.7 ($M_s=+1/2$) and between 0.5 and 0.0 ($M_s=-1/2$), depending on the orientation of $\mathbf{B}_2$.

6.5. ENDOR transition moments in powders. Calculating the squared transition moment W^2 in a powder sample requires integration of W^2 over angle ψ for each set of θ and φ. Angles θ and φ are the polar coordinates of **B**, and the angle ψ relates the orientation of the molecule to the RF field direction for each direction of **B**.[21] In a powder all molecules with the same orientation with respect to **B** will have the same resonance frequency, but they will be randomly oriented relative to $\mathbf{B}_2$. The variation in W with the orientation of $\mathbf{B}_2$ can be significant, as pointed out by several authors.[23,25,45] Although the effect of the RF orientation has been known for a long time it has, to the best of our knowledge, never been fully taken into account when calculating ENDOR transition moments in powders. Analytical integration of eqn. (30), over the distribution of $\mathbf{B}_2$ directions in the plane perpendicular to **B** gives the expression[23]

$$\bar{W}^2(\theta,\varphi)=\int_\psi W^2(\theta,\varphi,\psi)\,d\psi$$
$$=\frac{1}{2}\left(\frac{B_2}{B}\right)^2(\alpha^*C^2\alpha-\alpha^*C\ell\cdot\alpha C\ell) \qquad (34)$$

where α is a vector with the components $\langle h|I_x|k\rangle$, $\langle h|I_y|k\rangle$ and $\langle h|I_z|k\rangle$, and α^* is obtained by complex conjugation of the components. The nuclear index i has been dropped for simplicity. The integration is done in a similar fashion as done by Kottis and Lefebvre[5] for triplet state EPR spectra. Analytical integration avoids the need for a time consuming numerical integration of W^2 over ψ.

6.6. The ENDOR powder lineshape. The first-derivative powder lineshape at the ENDOR frequency f and static magnetic field B is approximated by the formula:[23]

$$\frac{d}{df}\chi(B,f)=\int_\theta \sin\theta\int_\varphi\sum_l\left[s(B-B_l)I_l^2\times\left(\frac{d}{df}\sum_k t(f-f_{lk})\bar{W}_{lk}^2\right)\right]d\varphi\,d\theta \qquad (35)$$

where

$$\bar{W}_{lk}^2=\int_\psi W_{lk}^2(\theta,\varphi,\psi)\,d\psi \qquad (36)$$

The summations run over the EPR transition fields $B_l(\theta,\phi)$ and the ENDOR transition frequencies $f_{lk}(\theta,\phi)$, with the corresponding transition moments $I_l(\theta,\phi)$ and $W_{lk}(\theta,\phi,\psi)$. Each nucleus with non-zero nqi gives rise to $(2I+1)^2$ EPR transitions and $2I(2I+1)$ possible ENDOR transitions. ENDOR transitions between all nuclear spin states within the same M_s-manifold of a nucleus are more or less allowed. Similarly EPR transitions between all initial and final nuclear spin states with different M_s-value are allowed. With zero nqi the number of ENDOR transitions reduces to $4I$ with the selection rule $\Delta Ms=0$, $\Delta m_I=\pm1$. Here m_I is the quantum number of the nuclear spin operator I_k along the nuclear quantization axis **k** given by eqn. (31). The EPR component lineshape function s acts as a weighting function. It selects the EPR transitions that contribute to the ENDOR signal at a particular field setting. Further we assume that only nuclear transitions which have an energy level in common with the EPR transitions that are in resonance will give an ENDOR response. The function t is a convolution function describing the lineshape of a specific ENDOR transition. The functions s and t can be selected as Lorentzian or Gaussian shaped. The integration over ψ is described above. Integration over θ and ϕ are performed using Gaussian quadrature as described in Ref. 4.

The structure of eqn. (35) can be derived from the general principles of powder ENDOR lineshapes outlined in Refs. 15 and 16 and is similar to eqn. (3) in Ref. 19, although we calculate transition moments W_{jk} to first

order and take into account the dependence of W_{jk} on the RF field direction, see eqns. (34) and (36). The intensity dependence in I_i due to g-anisotropy is neglected and we assume constant, isotropic linewidths for the lineshape functions. Neither spin relaxation nor instrumental effects on the lineshape are included in eqn. (35).

It should be noted here that the orientational selectivity depends on the ratio between the electron spin–spin relaxation rate (T_{xe}^{-1}) and the electron spin–lattice relaxation rate (T_{1e}^{-1}).[22] Orientational selectivity is efficient if $T_{xe}^{-1} \ll T_{1e}^{-1}$, which is the common situation for transition metal complexes and radicals in frozen solution above 77 K.[48] The ENDOR spectrum is then the sum of all transitions that are connected to the EPR transitions in resonance. In the other limit, when $T_{xe}^{-1} \gg T_{1e}^{-1}$, the ENDOR spectrum is the sum of all possible orientations irrespective of which part of the EPR spectrum that is monitored. This situation has been encountered for organic radicals at very low temperatures, $\leqslant 4$ K.[22,49]

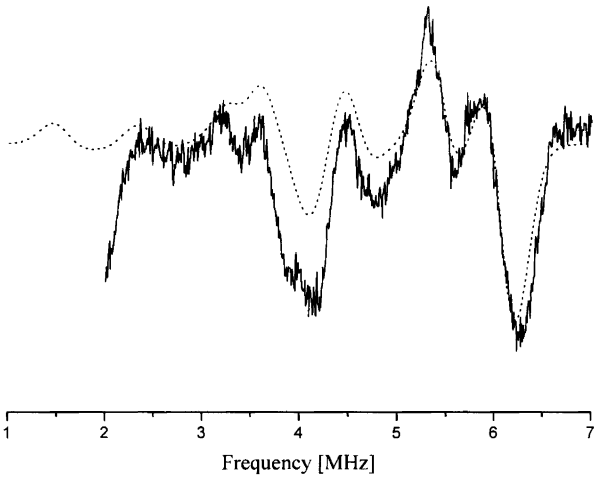

Fig. 5. Experimental (solid line) and simulated (dotted line) powder ENDOR spectra at 110 K of X-irradiated hippuric acid. Only the region of ^{14}N-signals is shown. The spectra were obtained at the centre of the EPR spectrum (Fig. 1) with microwave frequency 9.57367 GHz and $B = 3415.3$ G. Hyperfine and nuclear quadrupolar tensor parameters were taken from Refs. 23 and 30.

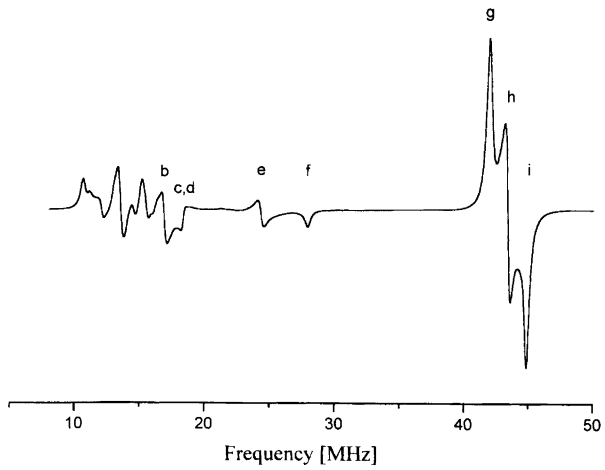

Fig. 6. Simulated powder ENDOR spectrum of the tyrosyl free radical in ribonucleotide reductase from *Escherichia coli*. Proton hyperfine tensor parameters were obtained from Ref. 49. Letters label line positions listed in Table 6.

This case is not implemented in eqn. (35), but has been treated for $I = 1/2$ nuclei by Dalton and Kwiram.[22]

The ENDOR program developed by us has been applied to simulate spectra of α-proton hyperfine couplings[13,14] as well as to spectra caused by ^{14}N-hyperfine and quadrupolar couplings.[23] Shown in Fig. 5 are experimental and simulated ENDOR spectra[23] of X-irradiated hippuric acid obtained at 110 K. Only the region of ^{14}N-signals is shown. The nitrogen nucleus has the principal hyperfine components: −7.58, -8.47, −9.44 MHz and quadrupolar components −0.843, +0.582, +0.261 Mhz.[23] ENDOR signals from α-proton hyperfine couplings in aromatic rings of π-radicals have been observed in a number of systems: biphenyl$^{\cdot+}$,[13] naphthalene$^{\cdot+}$,[14] perylene$^{\cdot+}$,[21] the tyrosyl radical[48] and *p*-benzoquinone$^{\cdot-}$.[50] In all these cases the hf tensors were anisotropic and the powder EPR spectra fairly unresolved. ENDOR simulation has proved to be essential in the interpretation of the spectra in several of these cases.[13,14,21] A simulation of the ENDOR spectrum of the tyrosyl free radical, R–$C_\beta H_2$–Ph$^{\cdot}$–O, in ribonucleotide reductase from *Escherichia coli* is shown in Fig. 6.

Table 6. Experimental and simulated powder ENDOR line positions for the tyrosyl free radical, R–$C_\beta H_2$–Ph$^{\cdot}$–O, in ribonucleotide reductase from *Escherichia coli*.

Transition[a]	Simulated line position/ MHz	Experimental line position[b]/ MHz	Proton[c]	Tensor component	Coupling constant
b	16.8	16.8	[2,6]-proton	A_1	4.8
c	18.2	18.2	[2,6]-proton	A_2	7.6
d	18.2	18.3	[3,5]-proton	A_y	−7.8
e	24.3	24.3	[3,5]-proton	A_z	−19.7
f	27.9	27.8	[3,5]-*proton*	A_x	−26.9
g	41.8	41.8	β-methylene	A_y	54.8
h	43.3	43.2	β-methylene	A_z	57.8
i	44.8	44.8	β-methylene	A_x	60.8

[a]For labeling refer to Fig. 6 of this work and Fig. 3 in Ref. 48. [b]See Table I in Ref. 48. [c]For proton labeling see Fig. 1 in Ref. 48.

Hyperfine parameters were taken from the experimental work by Bender *et al.*[48] The lineshape is caused by hyperfine couplings from α-protons on the tyrosyl phenol ring, $Ph^{\cdot}$, and β-protons on the β-carbon. The simulation corresponds to the experimental spectrum shown in Fig. 3 in Ref. 48. The agreement between experimental[48] and simulated line positions is excellent (Table 6). The simulation program written in Microsoft FORTRAN is available upon request to the authors. Details of the program can be found in Ref. 51.

7. Conclusions

Computer simulation using simple formulas calculated by perturbation theory may be one way to facilitate interpretation of complex powder EPR and ENDOR spectra. Although single-crystal samples may be preferred due to the higher spectral resolution offered, many samples cannot be obtained in other forms than powders. In these cases there are few alternatives but to attempt to elucidate as much information from the powder spectra as possible. The computer program developed by us to simulate $S=1/2$ and $S=1$ EPR and $S=1/2$ ENDOR spectra of anisotropic systems have been applied to analyse disordered systems with good performance.

Acknowledgements. The research has been financially supported by the Swedish Science Research Council (NFR). Prof. J. Michalik has kindly provided the spectrum of Ag_3^{2+} in zeolite shown in Fig. 2. The exact calculations of Table 2 were kindly provided by Prof. J. Hüttermann.

References

1. Kirste, B. In Poole, C. P. Jr. and Farach, H. A., Eds., *Handbook of Electron Spin Resonance*, Woodbury 1994, American Institute of Physics Press, pp. 27–50.
2. Pilbrow, J. R. *Transition Ion Electron Paramagnetic Resonance*, Clarendon Press, Oxford 1990, pp. 211–259, 646–647.
3. Mombourquette, M. J., Weil, J. A. and McGavin, D. G. *EPR-NMR User's Manual*, University of Saskatchewan, Canada 1996.
4. Lefebvre, R. and Maruani, J. *J. Chem. Phys. 42* (1965) 1480.
5. Kottis, P. and Lefebvre, R. *J. Chem. Phys. 39* (01963) 393.
6. Weber, R. T. *Win-EPR Sinfonia Manual*, Bruker Instruments, Inc. 1995.
7. Thuomas, K. A. and Lund, A. *J. Magn. Reson. 22* (1976) 315.
8. Lund, A., Thuomas, K-Å. and Maruani, J. *J. Magn. Reson. 30* (1978) 505.
9. Claesson, O., Lund, A., Gillbro, T., Ichikawa, T. and Yoshida, Y. *J. Chem. Phys.72* (1980) 1463.
10. Claesson, O. and Lund, A. *J. Magn. Reson. 41* (1980) 106.
11. Sagstuen, E., Hole, E. O., Haugedal, S. R., Lund, A., Eid, O. I. and Erickson, R. *Nukleonika. Accepted for publication.*
12. Rist, G. H. and Hyde, J. S. *J. Chem. Phys, 52* (1970) 4633.
13. Erickson, R., Lund, A. and Lindgren, M. *Chem. Phys. 193* (1995) 89.
14. Erickson, R., Benetis, N. P., Lund, A. and Lindgren, M. *J. Phys. Chem. A 101* (1997) 2390.
15. (a) Hoffman, B. M., Martinsen, J. and Venters, R. A. *J. Magn. Reson. 59* (1984) 110; (b) Hoffman, B. M., Venters, R. A. and Martinsen, J. *J. Magn. Reson. 62* (1985) 537; (c) Hoffman, B. M. and Gurbiel, R. J. *J. Magn. Reson. 82* (1989) 309.
16. (a) Hoffman, B. M., Gurbiel, R. J., Werst, M. M. and Sivaraja, M. In Hoff, E. J., Ed., *Advanced EPR: Applications in Biology and Biochemistry*, Elsevier, Amsterdam 1989, pp. 541–591; (b) Gurbiel, R. J., Batie, C. J., Sivaraja, M., True, A. E., Fee, J. A., Hoffman, B. M. and Ballou, D. P. *Biochemistry 28* (1989) 4861.
17. (a) Hurst, G. C., Henderson, T. A. and Kreilick, R. W. *J. Am. Chem. Soc. 107* (1985) 7294; (b) Henderson, T. A., Hurst, G. C. and Kreilick, R. W. *J. Am. Chem. Soc. 107* (1985) 7299.
18. Gochev, G. P. and Yordanov, N. D. *J. Magn. Reson. 102* (1993) 180.
19. Kreiter, A. and Hüttermann, J. *J. Magn. Reson. 93* (1991) 12.
20. Keijzers, C. P., Reijerse, E. J., Stam, P., Dumont, M. F. and Gribnau, M. C. M. *J. Chem. Soc., Faraday. Trans. 1, 83* (1987) 3493.
21. (a) Clarkson, R. B., Belford, R. L., Rothenberger, K. S. and Crookham, H. C. *J. Catal. 106* (1987) 500; (b) Rothenberger, K. S., Crookham, H. C., Belford, R. L. and Clarkson, R. B. *J. Catal. 115* (1989) 430; (c) Clarkson, R. B., Mattson, K., Shi, W., Wang, W. and Belford, R. L. In Lund, A. and Rhodes, C., Eds., *Radicals on Surfaces*, Kluwer, Dordrecht 1995, pp. 89–117.
22. Dalton, L. R. and Kwiram, A. L. *J. Chem. Phys. 57* (1972) 1132.
23. Erickson, R. *Chem. Phys. 202* (1996) 263.
24. Toriyama, K., Nunome, K. and Iwasaki, M. *J. Chem. Phys. 64* (1976) 348.
25. Schweiger, A. and Günthard, Hs. H. *Chem. Phys. 70* (1982) 1.
26. Rockenbauer, A. and Simon, P. *J. Magn. Reson. 11* (1973) 217.
27. Iwasaki, M. *J. Magn. Reson. 16* (1974) 417.
28. Weil, J. A. *J. Magn. Reson. 18* (1975) 113.
29. Erickson, R. and Lund, A. *J. Magn. Reson. 92* (1991) 146.
30. (a) Chacko, V. P., McDowell, C. A. and Singh, B. C. *J. Chem. Phys. 72* (1980) 4111; (b) Salih, N. A., Sanderud, A., Sagstuen, E., Eid, O. E. and Lund, A. *Chem. Phys. Submitted.*
31. (a) Fessenden, R. W. *J. Chem. Phys. 37* (1962) 747; (b) Maruani, J., Coope, J. A. R. and McDowell, C. A. *Molec. Phys. 18* (1970) 165.
32. van der Pol, A., Reijerse, E. J., de Boer, E., Wasowicz, T. and Michalik, J. *Mol. Phys. 75* (1992) 37.
33. Iwasaki, M., Minakata, K. and Toriyama, K. *J. Chem. Phys. 54* (1971) 3225.
34. *Triplet State ODMR Spectroscopy*, Clarke, R. H., Ed., John Wiley & Sons, New York 1982.
35. Nam, J. W. and Regulla, D. F. *Appl. Radiat. Isot. 40* (1989) 953.
36. Kuroda, S.-I. and Miyagawa, I. *J. Chem. Phys. 76* (1982) 3933.
37. Trammel, G. I., Zeldes, H. and Livingston, R. *Phys. Rev. 110* (1958) 630.
38. Maruani, J. *J. Magn. Reson. 7* (1972) 207.
39. Portis, A. M. *Phys. Rev. 91* (1953) 1071.
40. Castner, T. G. *Phys. Rev. 115* (1959) 1506.
41. Brustolon, M., Maniero, A. L., Jovine, S. and Segre, U. *Res. Chem. Intermed. 22* (1996) 359.
42. Atherton, N. M. *Principles of Electron Spin Resonance*, Ellis Horwood, Chichester, 1993.
43. Freed, J. H. In Dorio, M. M. and Freed, J. H., Eds., *Multiple Electron Resonance Spectroscopy*, Plenum Press, New York 1979, pp. 73–142.
44. (a)Brustolon, M., Cassol, T., Micheletti, L. and Segre, U.

Mol. Phys. 61 (1987) 249; (b) Brustolon, M., Maniero, A.-L. and Segre, U. *Mol. Phys. 65* (1988) 447.
45. Whiffen, D. H. *Mol. Phys. 10* (1966) 595.
46. Fujimoto, M., McDowell, C. A. and Takui, T. *J. Chem. Phys. 70* (1979) 3694.
47. Abragam, A. *The Principles of Nuclear Magnetism*, Clarendon Press, Oxford 1961.
48. Möbius, K. and Lubitz, W. In Berliner, L. J. and Reuben, J., Eds., *Biological Magnetic Resonance*, Vol. 7, Plenum, New York 1987, pp. 129–247.
49. Bender, C. J., Sahlin, M., Babcock, G. T., Barry, B. A., Chandrasekar, T. K., Salowe, S. P., Stubbe, J., Lindström, B., Pettersson, L., Ehrenberg, A. and Sjöberg, B.-M. *J. Am. Chem. Soc. 111* (1989) 8076.
50. O'Malley, P. J. and Babcock, G. T. *J. Am. Chem. Soc. 108* (1986) 3995.
51. Erickson, R. *Electron Magnetic Resonance of Free Radicals. Theoretical and Experimental EPR, ENDOR and ESEEM Studies of Radicals in Single Crystal and Disordered Solids*, Linköping Studies in Science and Technology, Dissertation No. 391 (1995) Linköping, Sweden.
52. Yoshida, H. and Edlund, G. *Chem. Phys. Lett. 42* (1976) 107.

Received April 7, 1997.